AIP | Journal of Applied Physics

Phase transitions and phase diagram of Ba(Zr0.2Ti0.8)O3-x(Ba0.7Ca0.3)TiO3 Pb-free system by anelastic measurement

Dezhen Xue, Jinghui Gao, Yumei Zhou, Xiangdong Ding, Jun Sun, Turab Lookman, and Xiaobing Ren

Citation: Journal of Applied Physics **117**, 124107 (2015); doi: 10.1063/1.4916713
View online: http://dx.doi.org/10.1063/1.4916713
View Table of Contents: http://scitation.aip.org/content/aip/journal/jap/117/12?ver=pdfcov
Published by the AIP Publishing

Phase transitions and phase diagram of $Ba(Zr_{0.2}Ti_{0.8})O_3$-$x(Ba_{0.7}Ca_{0.3})TiO_3$ Pb-free system by anelastic measurement

Dezhen Xue,[1,2] Jinghui Gao,[1,3] Yumei Zhou,[1,a)] Xiangdong Ding,[1] Jun Sun,[1] Turab Lookman,[2] and Xiaobing Ren[1,4]
[1]*Multi-disciplinary Materials Research Center, Frontier Institute of Science and Technology, State Key Laboratory for Mechanical Behavior of Materials, Xi'an Jiaotong University, Xi'an 710049, China*
[2]*Theoretical Division, Los Alamos National Laboratory, Los Alamos, New Mexico 87545, USA*
[3]*State Key Lab of Electrical Insulation and Power Equipment, Xi'an Jiaotong University, Xi'an 710049, China*
[4]*Ferroic Physics Group, National Institute for Materials Science, Tsukuba, 305-0047 Ibaraki, Japan*

(Received 11 December 2014; accepted 22 March 2015; published online 31 March 2015)

The internal friction and storage modulus of $Ba(Zr_{0.2}Ti_{0.8})O_3$-$x(Ba_{0.7}Ca_{0.3})TiO_3$ (BZT-xBCT) Pb-free ceramics have been measured by dynamic mechanical analysis. The anelastic properties show clear anomalies with regard to the transformations between cubic (C), tetragonal (T), orthorhombic (O), and rhombohedral (R) phases, which are all of ferroelastic in nature. The previous reported T-R transition region in the BZT-xBCT system can be divided into the T-O and O-R transitions, consistent with recent studies on the appearance of an intermediate O phase. Based on the internal friction and storage modulus results, a revisited version of BZT-xBCT phase diagram is proposed.
 [http://dx.doi.org/10.1063/1.4916713]

I. INTRODUCTION

Piezoelectric materials have the desirable property of energy conversion involving mechanical and electrical domains.[1,2] Amongst known piezoelectric materials, the lead oxide based compounds, for example, $PbZr_{1-x}Ti_xO_3$ (PZT), $PbMg_{1/3}Nb_{2/3}O_3$–xPbTiO$_3$ (PMN-PT), and $PbZn_{1/3}Nb_{2/3}O_3$–xPbTiO$_3$ (PZN-PT), are the current workhorses for a vast range of applications such as piezoelectric actuators, sensors, and transducers.[3–5] However, due to issues with lead toxicity, there is an urgent need for high performance lead-free alternatives.[6–8]

Liu and Ren previously reported that a $BaTiO_3$-based lead-free ferroelectric system, $Ba(Zr_{0.2}Ti_{0.8})O_3$–$x(Ba_{0.7}Ca_{0.3})TiO_3$ (hereafter abbreviated as BZT-xBCT), exhibits a large electro-mechanical response, with a d_{33} over 600 pC/N.[9,10] It is of potential interest as an alternative to lead-based systems as the phase diagram of BZT-xBCT was shown to be similar to that of PZT, PMN-PT, and PZN-PT, i.e., it consisted of three regions: paraelectric cubic (C), ferroelectric rhombohedral (R), and ferroelectric tetragonal (T).[9,10] The phase boundary separating R and T phases leads to a large instability in the polarization state, and consequently a significant variation of the polarization can result under external stress or electric field.[9,11,12] Furthermore, the R-T phase boundary originates from the triple point, which is also shown to be a tricritical point.[9,13–15] The second order phase transition nature at this point further leads to a more isotropically flattened energy profile so that the polarization can be easily rotated by external stress or electric field. Therefore, the longitudinal piezoelectric coefficient d_{33} in BZT-50BCT is reported to be about 620 pC/N.[9,10]

It is known that that there is no group-subgroup relationship between the ferroelectric R and T phases.[16–18] Various studies focus on how the ferroelectric T phase transforms smoothly to the ferroelectric R phase.[19–27] For example, neutron and X-ray diffraction investigations on PMN-PT, PZN-PT, PZT single crystals, and ceramics have shown the presence of an intermediate phase (IP) (can be either a monoclinic (M) or an orthorhombic (O) phase) linking T and R in the MPB region.[19,20] For the BZT-xBCT system, recent Rietveld refinement on high resolution X-ray diffraction results also suggest an O phase bridging the T and R phases and the phase sequence is identical to that observed in $BaTiO_3$, i.e., Tetragonal → Orthorhombic → Rhombohedral upon cooling.[28,29] Recent TEM observations on BZT-xBCT and PMN-PT ceramics further show that such an intermediate phase (IP) can be considered as a nano-scale adaptive phase of nano-regions with T and R symmetries.[25,27,30,31] Thus, the nature of the phase transition in BZT-xBCT remains an outstanding question to be carefully examined.

By far, the most commonly applied technique used to characterize the transition behavior is dielectric spectroscopy.[9,11,32,33] The dynamic response to an AC electric field gives the real part (ϵ') and the imaginary part (ϵ'') of the permittivity and their ratio is the dielectric loss, $\tan\delta = \frac{\epsilon'}{\epsilon''}$. However, because there is strong coupling between lattice distortions (strain) and the ferroelectric order parameter (polarization), it is inevitable that there will be changes in elastic and anelastic properties associated with the discrete phase transitions in the BZT-xBCT lead-free system.[34–36] The real part of the elastic response to a dynamic stress field, expressed as the storage modulus (E'), is the inverse of the mechanical susceptibility. The imaginary part of the response is the loss modulus (E''). And the mechanical loss (i.e., internal friction) is given by $Q^{-1} = \frac{E'}{E''}$. Softening of elastic storage modulus often appears near a structural

a)Electronic mail: zhouyumei@mail.xjtu.edu.cn.

ferroelectric phase transition, whereas the relaxation of order parameters, motion of phase boundaries, and nucleation of a new phase over the course of a phase transition typically give rise to an internal friction peak.[37] Therefore, mechanical spectroscopy provides additional insights into the structural evolution from a slightly different perspective.[36,38,39]

In the present study, we investigated the phase transition behavior of the $Ba(Zr_{0.2}Ti_{0.8})O_3$–$x(Ba_{0.7}Ca_{0.3})TiO_3$ (BZT-xBCT) Pb-free polycrystalline system using dynamic mechanical analysis (DMA). The storage modulus and mechanical loss showed clear anomalies in the transformation process between the cubic (C), tetragonal (T), and rhombohedral (R) phases and the intermediate phase (IP). The previously reported T-R transition region in the BZT-xBCT system can be divided into T-IP and IP-R transitions, consistent with a recently reported appearance of an intermediate orthorhombic (O) phase.[28,33,40] Based on our internal friction and storage modulus results, we revisited the structural phase diagram of the BZT-xBCT system, which is consistent with the ones reported recently.[28,40,41] Our results suggest that the measurement of anelastic properties provides a suitable approach to monitor the phase transition in piezoelectric systems, especially the $BaTiO_3$ based systems.

II. EXPERIMENT

BZT-xBCT ceramics with $0.20 \leq x \leq 0.45$ were fabricated by the conventional solid-state reaction method using starting chemicals $BaZrO_3$ (98%), $CaCO_3$ (99.9%), $BaCO_3$ (99.95%), and TiO_2 (99.9%). The calcination was performed at 1350 °C, and sintering was done at 1450 °C in air. The sintered samples for dielectric measurement were polished to obtain parallel sides and painted with silver electrodes. The dielectric permittivity and dielectric loss were evaluated using a HIOKI3532 LCR meter at different frequencies (0.1/1/10/100 kHz). The sintered samples for anelastic measurement were cut into rectangular shapes of dimensions $1.0 \times 2.0 \times 20\,mm^3$. The storage modulus and mechanical loss were measured by DMA measurement in a three point bending mode. Such dynamic mechanical properties as a function of temperature were measured at different frequencies (0.2/0.4/1/4/10 Hz) with a constant displacement amplitude of 5 μm (the corresponding strain amplitudes were 0.57×10^{-3}).

III. RESULTS

A. The transition behavior in the composition region with transition sequence cubic → rhombohedral

Figure 1 shows the dielectric permittivity (ϵ'), dielectric loss ($\tan\delta$), elastic storage modulus (E'), and mechanical losses (Q^{-1}) for BZT-xBCT samples in the composition region with transition sequence cubic → rhombohedral during cooling. Peaks in both dielectric and anelastic properties are clearly visible around 330 K and 337 K for BZT-20BCT and BZT-25BCT, respectively. The frequency independent peaks in the dielectric permittivity and in dielectric loss correspond to the paraelectric-ferroelectric phase transition (T_c) from cubic to rhombohedral phase. As the transition is also coupled with the lattice distortion, there exists a sharp elastic storage

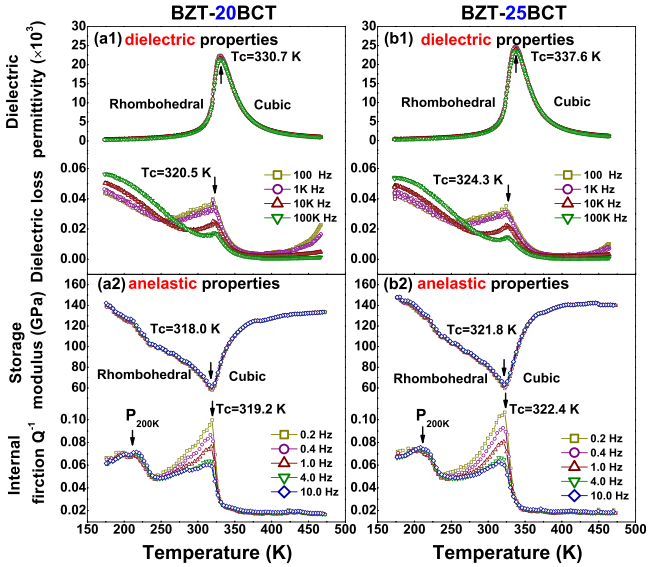

FIG. 1. The temperature dependence of dielectric permittivity (ϵ'), dielectric loss ($\tan\delta$), elastic storage modulus (E'), and mechanical loss (Q^{-1}) for (a) BZT-20BCT and (b) BZT-30BCT samples during cooling.

modulus dip and mechanical loss peak at T_c. Another anomaly, which is barely discernible in the storage modulus E', is clearly seen in mechanical loss Q^{-1} around 200 K, as indicated by P_{200K} in Fig. 1. In the dielectric loss $\tan\delta$, the corresponding anomaly is located at even lower temperature. Some frequency dependence of the peaks in dielectric loss ($\tan\delta$) and mechanical loss (Q^{-1}) can be observed. The P_{200K} peak is attributed to the relaxation of domain walls and will be discussed later in the discussion part.

B. The transition behavior in the composition interval with transition sequence cubic → tetragonal → intermediate phase → rhombohedral

With higher x, the transition sequence is modified from a one step transition to multi-step transitions. The dielectric permittivity (ϵ'), dielectric loss ($\tan\delta$), elastic storage modulus (E'), and mechanical loss (Q^{-1}) as a function of temperature for BZT-xBCT samples with $x = 35$, 40, 45 are shown in Fig. 2. These samples transform from cubic to tetragonal, through the intermediate phase, and finally to the rhombohedral phase. Several anomalies in both dielectric and anelastic properties can be seen in the three BZT-35BCT, BZT-40BCT, and BZT-45BCT samples. As shown by the dashed line in Fig. 2, the temperature axis can be divided into four regions by three anomalies at different temperatures. The frequency independent peaks in the dielectric permittivity and in dielectric loss on the high temperature side correspond to the paraelectric to ferroelectric phase transition (T_c) from paraelectric cubic to ferroelectric tetragonal phase as shown in Figs. 2(a1)–2(c1). Similar to the transition from cubic to rhombohedral in Fig. 1, there exists in addition an elastic storage modulus dip and a mechanical loss peak at T_c (as shown in Figs. 2(a2)–2(c2)). With decreasing temperature, the dip in elastic storage modulus and the peak in mechanical loss increase. Meanwhile, there exists a peak in the dielectric loss but only a bump in the dielectric permittivity at this temperature. These anomalies

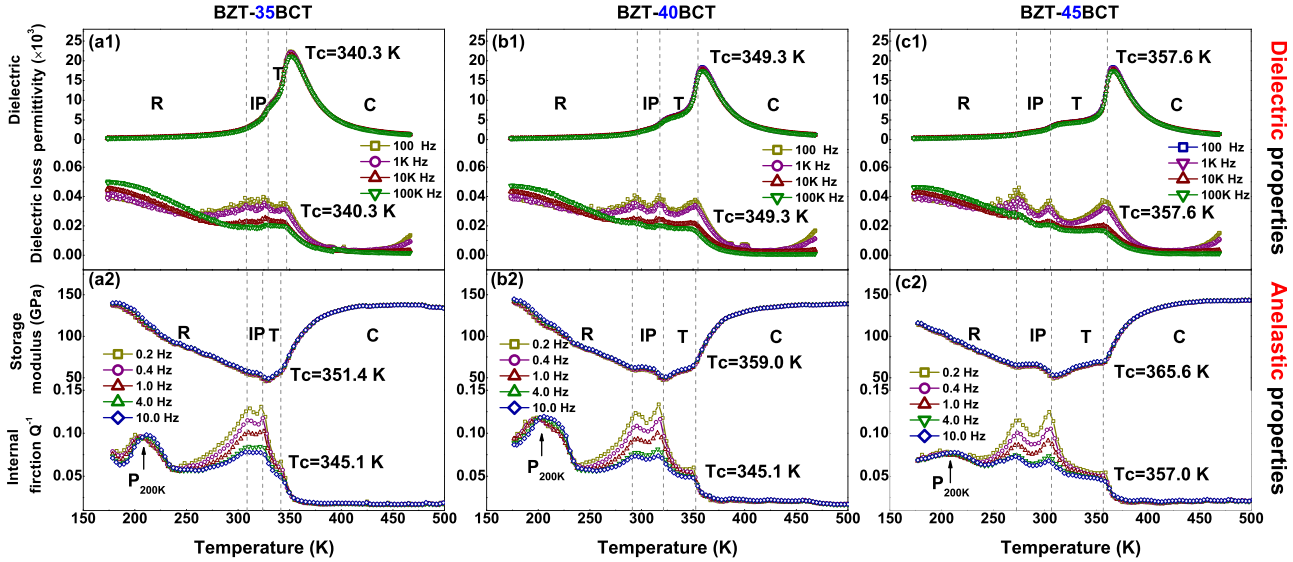

FIG. 2. The temperature dependence of dielectric permittivity (ϵ), dielectric loss ($\tan\delta$), elastic storage modulus (E'), and mechanical loss (Q^{-1}) for (a) BZT-35BCT (b) BZT-40BCT and (c) BZT-45BCT samples during cooling.

correspond to the transition from a tetragonal phase to an intermediate phase (T_{T-IP}). We note that such a phase transition strongly affects the anelastic properties but is not mirrored in the dielectric response. Such decoupling between anelastic and dielectric properties may be the result of the fact that the change of strain at this transition is more significant than that of polarization. With further decrease of temperature, the intermediate phase transforms into the rhombohedral phase at T_{IP-R}, resulting in a small dip in elastic storage modulus and a fairly high mechanical loss peak. The anomaly in dielectric properties at this transition T_{IP-R} is more obvious in dielectric loss (a peak) but almost invisible in dielectric permittivity. In the rhombohedral phase, there exists a mechanical loss peak around 200 K (as noted by P_{200K}) due to relaxation processes, as well as a broad dielectric loss peak at even lower temperature.

C. The transformation behavior in the composition region close to the triple point

Figure 3 further shows the dielectric permittivity (ϵ'), dielectric loss ($\tan\delta$), elastic storage modulus (E'), and mechanical loss (Q^{-1}) for BZT-xBCT samples in the composition region close to the triple point where that paraelectric cubic, ferroelectric tetragonal, rhombohedral, and intermediate phases coexist. The compositions near the triple point represent the crossover between the two regions shown in Figs. 1 and 2. Three BZT-xBCT samples with $x = 30, 32, 33$ were investigated. Only one anomaly was found close to 350 K in dielectric permittivity and elastic storage modulus. The mechanical loss and dielectric loss show a transition peak on the high temperature side and there is also a broad relaxation peak located around 200 K. This is similar to the transition behavior in the composition region with transition

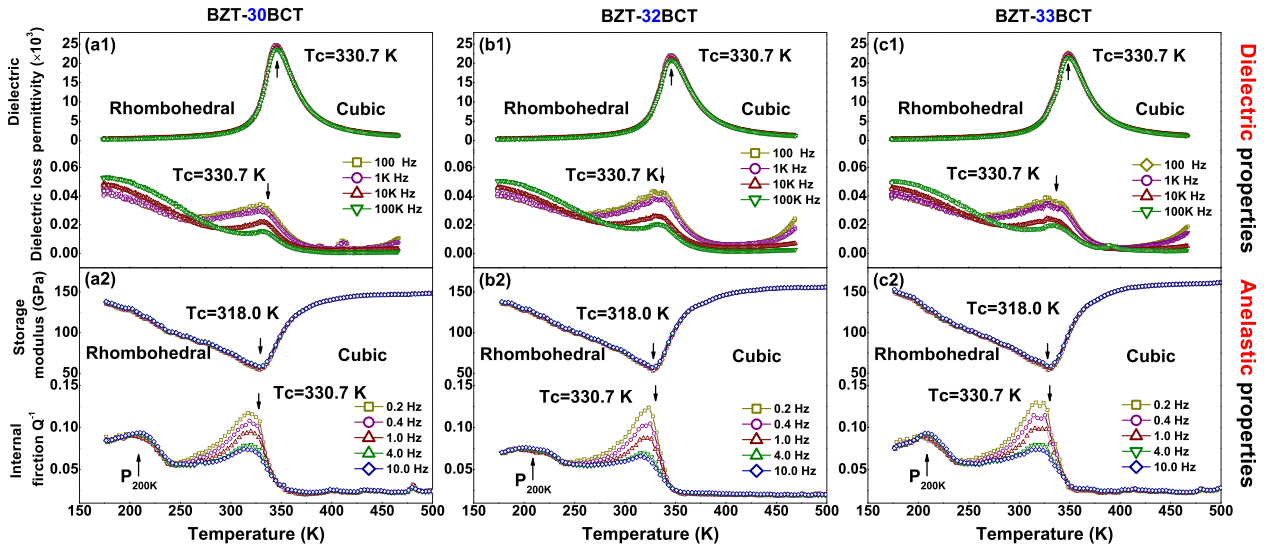

FIG. 3. The temperature dependence of dielectric permittivity (ϵ), dielectric Loss ($\tan\delta$), elastic storage modulus (E'), and mechanical loss (Q^{-1}) of BZT-30BCT (a), BZT-32BCT (b), and BZT-33BCT (c) samples during cooling.

sequence cubic → rhombohedral, shown in Subsection III A. However, the peak and dip are broader here, and more importantly, the dielectric permittivity at the transition peak is higher and storage modulus lower than at the composition $x = 20, 25$ in Fig. 1.

D. Phase diagram for BZT-*x*BCT system

Figure 4 shows the phase diagram for the BZT-*x*BCT system deduced from the present anelastic (1 Hz) measurements, together with the dielectric measurements (1 kHz). The anomalies distinguishing the IP from T and R phases have been reported by Damjanovic *et al.*, where inflection points can be identified in the storage and loss modulus of BZT-50BCT.[36] Good agreement was found for the phase transition temperatures obtained from anelastic measurements with those from dielectric measurements, diffraction, and Raman scattering.[9,11,28,33,40,41] However, the origin of the intermediate phase between the R and T phases is still uncovered. Liu and Ren considered a single phase boundary separating R and T, while TEM work by Gao *et al.* suggested a T and R coexisted region.[9,27] Recent Rietveld refinement on high resolution X-ray diffraction results also suggest an orthorhombic (Amm2) phase bridging the T and R phases.[28] The BZT-*x*BCT phase diagram here includes an intermediate phase; consequently the tetragonal to rhombohedral phase boundary was divided into the T-IP and IP-R phase boundaries, consistent with recent reports on the presence of an intermediate orthorhombic phase.[28,33,40,41] The two T-IP and IP-T phase boundaries are marked by blue and red lines, respectively, in Fig. 4. The phase transition sequence at MPB follows C-T-IP-R during cooling, not the same as Liu and Ren reported, i.e., C-T-R.[28,33,40,41]

Comparing with the anomalies in the dielectric properties, the ones in the anelastic properties seem more distinct, especially in the internal friction. The same situation can also be found in the anelastic measurement of PZT and $(Na_{0.5}Bi_{0.5})_{1-x}Ba_xTiO_3$ (NBT-BT) systems.[38,42] However, the reason for this is still unclear and one possibility is that the energy is dissipated more upon mechanical excitation at the ferroelectric-ferroelectric transitions. But the exact reason still needs further studies. Anyhow, it seems that the measurement of anelastic properties (storage modulus, internal friction, etc.) provides a suitable approach to determining the phase transitions in piezoelectric materials.

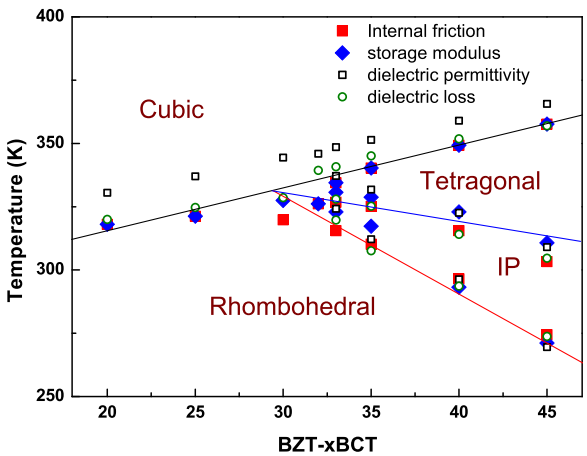

FIG. 4. Phase diagram for BZT-*x*BCT deduced from the present anelastic (at 1 Hz) and dielectric 1 kHz measurements. C=cubic, T = tetragonal, R = rhombohedral, IP = intermediate phase. Solid lines are a guide to the eye.

IV. DISCUSSION

A. The elastic softening at the triple point

It has already been shown that the triple point in the phase diagram of BZT-*x*BCT corresponds to a very soft state of polarization and thus can enable easy polarization rotation.[12,39] This is also supported by the fact that the BZT-30BCT, a triple-point composition, exhibits the highest permittivity peak at T_c compared to that for the off-triple-point compositions, as shown in Figs. 1–3. Thus, there exists a strong polarization softening at the triple point. As the material is strongly electromechanically coupled, there should exist a strong elastic softening as well.[10] Besides the softness in polarization, elastic softening plays an important role in the high piezoelectricity regime at the MPB.[39] Therefore, in the present study, we compared the elastic storage modulus softening at the paraelectric to ferroelectric transition temperature, T_c. The elastic storage modulus as a function of temperature for BZT-*x*BCT ($0.20 \leq x \leq 0.45$) samples is presented in Fig. 5. In order to compare the lattice softening during the transition, the elastic modulus of each composition is normalized by its own elastic modulus value at 150 °C, respectively. As can be seen in Fig. 5(a), the phase transitions, including T_c, T_{T-IP}, and T_{IP-R}, are all characterized by a dip in elastic storage modulus. Here, we focus on the paraelectric to ferroelectric transition only as we would like to observe the anomaly of the triple point. The elastic storage modulus at T_c (paraelectric to ferroelectric transition temperature) drops by different amounts as a function of composition x, compared to the elastic modulus of the paraelectric phase. Figure 5(b) thus shows the composition x

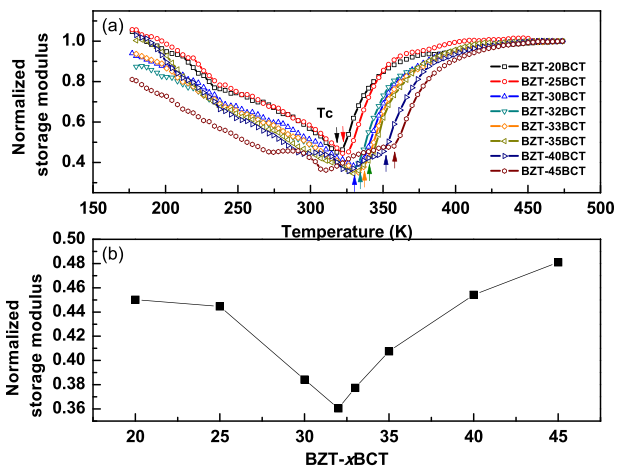

FIG. 5. (a) Elastic storage modulus of BZT-xBCT for $0.20 \leq x \leq 0.45$ as a function of temperature. These curves are normalized by their corresponding elastic storage modulus at 450 K. The elastic storage modulus is for frequency 1 Hz. (b) The relative drop of elastic modulus at the paraelectric to ferroelectric transition temperature, T_c, with respect to the elastic modulus in the paraelectric phase (450 K).

dependence of such softening. The elastic storage modulus shows the lowest value near the triple point composition, corresponding to an elastically "soft" state near the triple point. Thus, at the triple point, the system is both electrically and elastically soft.

B. The composition dependence of internal friction at the transitions

It is generally believed that the larger energy dissipation during the course of the phase transition leads to an increase in internal friction and can decrease piezoelectric properties. Figure 6 shows the composition dependence of the internal friction at the cubic to tetragonal, tetragonal to IP, and IP to rhombohedral transitions.

It is known that the internal friction peak at a phase transition, especially for low frequency (<10Hz) measurements, is due to the influence of phase boundaries resulting from the nucleation and growth of a new phase. Thus, the low-frequency internal friction is related to the transformation volume and is thus proportional to the heating rate $\frac{dT}{dt}$ and the reciprocal of the measurement frequency f. The internal friction associated with the phase transition is then given by[37]

$$Q^{-1} = \frac{\Delta\bar{J}}{\bar{J}} \frac{dM(T)}{dT} \frac{dT}{dt} \omega^{-1}, \tag{1}$$

where $\Delta\bar{J}$ is the average change of the compliance due to the phase transition, $\bar{J}$ is the average compliance of the material, $M(T)$ is the volume fraction that has transformed to a new phase at the temperature T, and $\omega = 2\pi f$. Equation (1) shows that the internal friction is inversely proportional to the frequency and explains the different internal friction peaks at the transition for different frequencies in Figs. 1–3. For a given frequency (for example, 1 Hz in Fig. 6), the $\frac{dM(T)}{dT}\frac{dT}{dt}\omega^{-1}$ terms can be considered as constants and the internal friction is then only proportional to the elastic compliance. Therefore, the larger change in elastic compliance $\Delta\bar{J}$ results in higher internal friction.

It can be seen in Fig. 6 that the internal friction associated with the paraelectric to ferroelectric transition (T_c) shows a peak near the triple point ($x = 30$). As shown in Fig. 5, it is known that the elastic storage modulus drops most dramatically close to $x = 30$, thus the elastic compliance change $\Delta\bar{J}$ is greatest there. According to Eq. (1), the internal friction is proportional to $\Delta\bar{J}$, thus there is peak at $x = 30$. This explains the internal friction anomaly near $x = 30$ in Fig. 6 and is consistent with the fact that the material is elastically very soft at the triple point ($x = 30$). Furthermore, we note that the internal friction at the T-IP and IP-R phase transitions decrease almost monotonically with the increase of x. This can be understood in the same way. From Fig. 5(a), it can be found that the elastic storage modulus at T_{T-IP} and T_{IP-R} increases with increasing x, thus $\Delta\bar{J}$ decrease with x. According to Eq. (1), internal friction drops with increasing x. And we also noted that internal friction at T_{T-IP} and T_{IP-R} is much higher than that at T_c for the same composition x, as shown in Fig. 6. This may be due to the larger change in elastic compliance $\Delta\bar{J}$ at those transitions compared to the C-T phase transition.

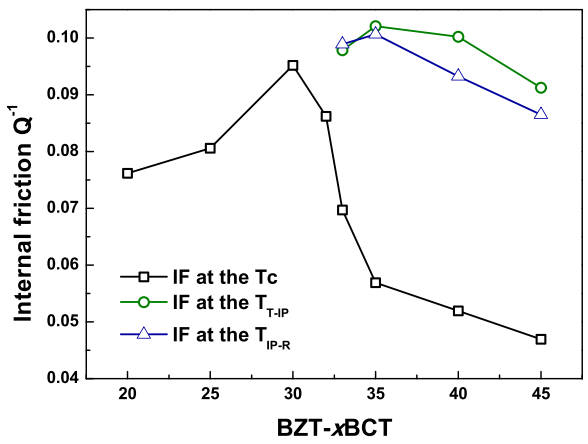

FIG. 6. Measured internal friction for cubic to tetragonal, tetragonal to intermediate phase, and intermediate phase to rhombohedral transitions as a function of composition x for the BZT-xBCT system.

C. The low temperature internal friction peak

The BZT-xBCT samples show an extra internal friction peak at low temperature near 200 K, as indicated by P_{200K} in Figs. 1–3. This is in addition to the internal friction peaks associated with the phase transitions from C-T, T-IP, and IP-R. The low temperature peaks are frequency dependent and thus a signature of the relaxation processes. If we assume the relaxation process to be thermally activated, then the activation parameters may be found using the Arrhenius relation

$$\tau = \tau_0 \exp\left(\frac{H}{k_B T}\right), \tag{2}$$

where τ is the relaxation time, H is the activation energy, k_B is the Boltzmann constant, and (τ_0) is the intrinsic relaxation time limit. Using $\omega = 2\pi f$, we have

$$\frac{1}{2\pi f} = \tau_0 \exp\left(\frac{H}{k_B T}\right). \tag{3}$$

The activation energy associated with the relaxation peak P_{200K} was determined to be 0.73 ± 0.15 eV for BZT-35BCT and 0.55 ± 0.16 eV for BZT-40BCT, which are comparable to the reported activation energy for interactions between domain walls and oxygen vacancies in ferroelectric phases.[43,44] Such a peak due to domain wall motion has already been observed in many ferroelectric materials, such as Pb-based PZT and Pb-free $BaTiO_3$ by anelastic measurement.[44] Thus, we suggest that the relaxation peak P_{200K} is the result of the interaction between domain wall motion and diffusion of oxygen vacancies in the BZT-xBCT samples.

V. SUMMARY

We have measured the anelastic properties, i.e., the internal friction (Q^{-1}) and storage modulus (E') for $Ba(Zr_{0.2}Ti_{0.8})O_3$–$x(Ba_{0.7}Ca_{0.3})TiO_3$ Pb-free ceramics by DMA. As the transformations in this class of materials are all ferroelastic in nature, mechanical loss peaks, and elastic storage modulus anomalies associated with the transitions are observed. Our results suggest that measurements of anelastic properties

(storage modulus, internal friction, etc.) provide a suitable approach to monitor and determine the phase transitions in piezoelectric materials. The previous reported T-R transition region in the BZT-*x*BCT system can be divided into the T-IP and IP-R transitions by our anelastic measurement, consistent with the recent reports.[28,33,40,41] We find that near the triple point the elastic behavior is very softest and the internal friction very large. Moreover, near 200 K in all the BZT-*x*BCT samples, we infer the presence of relaxation processes controlled by domain wall motions.

ACKNOWLEDGMENTS

The authors gratefully acknowledge the support of National Basic Research Program of China (Grant No. 2012CB619401), the National Natural Science Foundation of China (Grant Nos. 51302209, 51207121, 51431007, 51201126, 51320105014, and 51321003), and 111 project of China (B06025). We are also grateful to the LDRD program at Los ALamos National Laboratory for support.

[1]M. E. Lines and A. M. Glass, *Principles and Applications of Ferroelectrics and Related Materials* (Clarendon Press, Oxford, 2001).
[2]K. Uchino, *Ferroelectric Devices* (CRC Press, 2000), Vol. 16.
[3]B. Jaffe, *Piezoelectric Ceramics* (Elsevier, 2012), Vol. 3.
[4]D. Cox, B. Noheda, G. Shirane, Y. Uesu, K. Fujishiro, and Y. Yamada, "Universal phase diagram for high-piezoelectric perovskite systems," Appl. Phys. Lett. **79**, 400–402 (2001).
[5]S. Zhang, F. Li, X. Jiang, J. Kim, J. Luo, and X. Geng, "Advantages and challenges of relaxor-$PbTiO_3$ ferroelectric crystals for electroacoustic transducers—a review," Prog. Mater. Sci. **68**, 1–66 (2014).
[6]Y. Saito, H. Takao, T. Tani, T. Nonoyama, K. Takatori, T. Homma, T. Nagaya, and M. Nakamura, "Lead-free piezoceramics," Nature **432**, 84–87 (2004).
[7]T. R. Shrout and S. J. Zhang, "Lead-free piezoelectric ceramics: Alternatives for PZT?," J. Electroceram. **19**, 113–126 (2007).
[8]J. Rödel, W. Jo, K. T. Seifert, E.-M. Anton, T. Granzow, and D. Damjanovic, "Perspective on the development of lead-free piezoceramics," J. Am. Ceram. Soc. **92**, 1153–1177 (2009).
[9]W. Liu and X. Ren, "Large piezoelectric effect in Pb-free ceramics," Phys. Rev. Lett. **103**, 257602 (2009).
[10]D. Xue, Y. Zhou, H. Bao, C. Zhou, J. Gao, and X. Ren, "Elastic, piezoelectric, and dielectric properties of $Ba(Zr_{0.2}Ti_{0.8})O_3$-$50(Ba_{0.7}Ca_{0.3})TiO_3$ Pb-free ceramic at the morphotropic phase boundary," J. Appl. Phys. **109**, 054110 (2011).
[11]D. Xue, Y. Zhou, J. Gao, X. Ding, and X. Ren, "A comparison between tetragonal-rhombohedral and tetragonal-orthorhombic phase boundaries on piezoelectricity enhancement," Europhys. Lett. **100**, 17010 (2012).
[12]A. A. Heitmann and G. A. Rossetti, "Thermodynamics of ferroelectric solid solutions with morphotropic phase boundaries," J. Am. Ceram. Soc. **97**, 1661–1685 (2014).
[13]H. Bao, C. Zhou, D. Xue, J. Gao, and X. Ren, "A modified lead-free piezoelectric BZT–xBCT system with higher TC," J. Phys. D: Appl. Phys. **43**, 465401 (2010).
[14]D. Xue, Y. Zhou, H. Bao, J. Gao, C. Zhou, and X. Ren, "Large piezoelectric effect in Pb-free $Ba(Ti,Sn)O_3$-x$(Ba,Ca)TiO_3$ ceramics," Appl. Phys. Lett. **99**, 122901 (2011).
[15]C. Zhou, W. Liu, D. Xue, X. Ren, H. Bao, J. Gao, and L. Zhang, "Triple-point-type morphotropic phase boundary based large piezoelectric Pb-free material–$Ba(Ti_{0.8}Hf_{0.2})O_3$-$(Ba_{0.7}Ca_{0.3})TiO_3$," Appl. Phys. Lett. **100**, 222910 (2012).
[16]M. Ahart, M. Somayazulu, R. Cohen, P. Ganesh, P. Dera, H.-k. Mao, R. J. Hemley, Y. Ren, P. Liermann, and Z. Wu, "Origin of morphotropic phase boundaries in ferroelectrics," Nature **451**, 545–548 (2008).
[17]A. Glazer, P. Thomas, K. Baba-Kishi, G. Pang, and C. Tai, "Influence of short-range and long-range order on the evolution of the morphotropic phase boundary in $Pb(Zr_{1-x}Ti_x)O_3$," Phys. Rev. B **70**, 184123 (2004).
[18]T. T. Lummen, Y. Gu, J. Wang, S. Lei, F. Xue, A. Kumar, A. T. Barnes, E. Barnes, S. Denev, A. Belianinov *et al.*, "Thermotropic phase boundaries in classic ferroelectrics," Nat. Commun. **5**, 3172 (2014).
[19]R. Guo, L. Cross, S. Park, B. Noheda, D. Cox, and G. Shirane, "Origin of the high piezoelectric response in $PbZr_{1-x}Ti_xO_3$," Phys. Rev. Lett. **84**, 5423 (2000).
[20]B. Noheda, D. Cox, G. Shirane, R. Guo, B. Jones, and L. Cross, "Stability of the monoclinic phase in the ferroelectric perovskite $PbZr_{1-x}Ti_xO_3$," Phys. Rev. B **63**, 014103 (2000).
[21]Y. Jin, Y. Wang, A. Khachaturyan, J. Li, and D. Viehland, "Adaptive ferroelectric states in systems with low domain wall energy: Tetragonal microdomains," J. Appl. Phys. **94**, 3629–3640 (2003).
[22]Y. Jin, Y. Wang, A. Khachaturyan, J. Li, and D. Viehland, "Conformal miniaturization of domains with low domain-wall energy: Monoclinic ferroelectric states near the morphotropic phase boundaries," Phys. Rev. Lett. **91**, 197601 (2003).
[23]F. Bai, J. Li, and D. Viehland, "Domain hierarchy in annealed (001)-oriented $Pb(Mg_{1/3}Nb_{2/3})O_3$-x%$PbTiO_3$ single crystals," Appl. Phys. Lett. **85**, 2313–2315 (2004).
[24]H. Wu, D. Xue, D. Lv, J. Gao, S. Guo, Y. Zhou, X. Ding, C. Zhou, S. Yang, Y. Yang *et al.*, "Microstructure at morphotropic phase boundary in $Pb(Mg_{1/3}Nb_{2/3})O_3$-$PbTiO_3$ ceramic: Coexistence of nano-scaled {110}-type rhombohedral twin and {110}-type tetragonal twin," J. Appl. Phys. **112**, 052004 (2012).
[25]J. Gao, L. Zhang, D. Xue, T. Kimoto, M. Song, L. Zhong, and X. Ren, "Symmetry determination on Pb-free piezoceramic $0.5Ba(Zr_{0.2}Ti_{0.8})O_3$-$0.5(Ba_{0.7}Ca_{0.3})TiO_3$ using convergent beam electron diffraction method," J. Appl. Phys. **115**, 054108 (2014).
[26]Y. Zhang, D. Xue, H. Wu, X. Ding, T. Lookman, and X. Ren, "Adaptive ferroelectric state at morphotropic phase boundary: Coexisting tetragonal and rhombohedral phases," Acta Mater. **71**, 176–184 (2014).
[27]J. Gao, D. Xue, Y. Wang, D. Wang, L. Zhang, H. Wu, S. Guo, H. Bao, C. Zhou, W. Liu *et al.*, "Microstructure basis for strong piezoelectricity in Pb-free $Ba(Zr_{0.2}Ti_{0.8})O_3$-$(Ba_{0.7}Ca_{0.3})TiO_3$ ceramics," Appl. Phys. Lett. **99**, 092901 (2011).
[28]D. S. Keeble, F. Benabdallah, P. A. Thomas, M. Maglione, and J. Kreisel, "Revised structural phase diagram of $(Ba_{0.7}Ca_{0.3}TiO_3)$-$(BaZr_{0.2}Ti_{0.8}O_3)$," Appl. Phys. Lett. **102**, 092903 (2013).
[29]J. Wu, A. Habibul, X. Cheng, X. Wang, and B. Zhang, "Orthorhombic–tetragonal phase coexistence and piezoelectric behavior in (1-x)$(Ba,Ca)(Ti,Sn)O_3$-x$(Ba,Ca)(Ti,Zr)O_3$ lead-free ceramics," Mater. Res. Bull. **48**, 4411–4414 (2013).
[30]H. Guo, C. Zhou, X. Ren, and X. Tan, "Unique single-domain state in a polycrystalline ferroelectric ceramic," Phys. Rev. B **89**, 100104 (2014).
[31]H. Guo, B. K. Voas, S. Zhang, C. Zhou, X. Ren, S. P. Beckman, and X. Tan, "Polarization alignment, phase transition, and piezoelectricity development in polycrystalline $0.5Ba(Zr_{0.2}Ti_{0.8})O_3$-$0.5(Ba_{0.7}Ca_{0.3})TiO_3$," Phys. Rev. B **90**, 014103 (2014).
[32]M. Acosta, N. Novak, W. Jo, and J. Rödel, "Relationship between electromechanical properties and phase diagram in the $Ba(Zr_{0.2}Ti_{0.8})O_3$-x$(Ba_{0.7}Ca_{0.3})TiO_3$ lead-free piezoceramic," Acta Mater. **80**, 48–55 (2014).
[33]Y. Tian, X. Chao, L. Jin, L. Wei, P. Liang, and Z. Yang, "Polymorphic structure evolution and large piezoelectric response of lead-free $(Ba,Ca)(Zr,Ti)O_3$ ceramics," Appl. Phys. Lett. **104**, 112901 (2014).
[34]M. C. Ehmke, F. H. Schader, K. G. Webber, J. Rödel, J. E. Blendell, and K. J. Bowman, "Stress, temperature, and electric field effects in the lead-free $(Ba,Ca)(Ti,Zr)O_3$ piezoelectric system," Acta Mater. **78**, 37–45 (2014).
[35]Y. Zhang, J. Glaum, C. Groh, M. C. Ehmke, J. E. Blendell, K. J. Bowman, and M. J. Hoffman, "Correlation between piezoelectric properties and phase coexistence in $(Ba,Ca)(Ti, Zr)O_3$ ceramics," J. Am. Ceram. Soc. **97**, 2885–2891 (2014).
[36]D. Damjanovic, A. Biancoli, L. Batooli, A. Vahabzadeh, and J. Trodahl, "Elastic, dielectric, and piezoelectric anomalies and Raman spectroscopy of $0.5Ba(Ti_{0.8}Zr_{0.2})O_3$-$0.5(Ba_{0.7}Ca_{0.3})TiO_3$," Appl. Phys. Lett. **100**, 192907 (2012).
[37]F. Yan, P. Bao, J. Zhu, Y. Wang, H. L. Chan, and C. L. Choy, "Phase transitions in $Pb(Mg_{1/3}Nb_{2/3})O_3$–$PbTiO_3$ studied by low-frequency internal friction measurement," J. Am. Ceram. Soc. **90**, 3167–3170 (2007).
[38]A. Bouzid, E. Bourim, M. Gabbay, and G. Fantozzi, "PZT phase diagram determination by measurement of elastic moduli," J. Eur. Ceram. Soc. **25**, 3213–3221 (2005).
[39]F. Cordero, F. Craciun, M. Dinescu, N. Scarisoreanu, C. Galassi, W. Schranz, and V. Soprunyuk, "Elastic response of (1x)$Ba(Ti_{0.8}Zr_{0.2})O_3$-

x($Ba_{0.7}Ca_{0.3}$)TiO_3 (x = 0.45–0.55) and the role of the intermediate orthorhombic phase in enhancing the piezoelectric coupling," Appl. Phys. Lett. **105**, 232904 (2014).
[40]L. Zhang, M. Zhang, L. Wang, C. Zhou, Z. Zhang, Y. Yao, L. Zhang, D. Xue, X. Lou, and X. Ren, "Phase transitions and the piezoelectricity around morphotropic phase boundary in $Ba(Zr_{0.2}Ti_{0.8})O_3$-x($Ba_{0.7}Ca_{0.3}$)TiO_3 lead-free solid solution," Appl. Phys. Lett. **105**, 162908 (2014).
[41]D. R. Brandt, M. Acosta, J. Koruza, and K. G. Webber, "Mechanical constitutive behavior and exceptional blocking force of lead-free BZT-xBCT piezoceramics," J. Appl. Phys. **115**, 204107 (2014).
[42]F. Cordero, F. Craciun, F. Trequattrini, E. Mercadelli, and C. Galassi, "Phase transitions and phase diagram of the ferroelectric perovskite $(Na_{0.5}Bi_{0.5})$(1-x)Ba_xTio_3 by anelastic and dielectric measurements," Phys. Rev. B **81**, 144124 (2010).
[43]E. M. Bourim, H. Tanaka, M. Gabbay, G. Fantozzi, and B. L. Cheng, "Domain wall motion effect on the anelastic behavior in lead zirconate titanate piezoelectric ceramics," J. Appl. Phys. **91**, 6662–6669 (2002).
[44]B. L. Cheng, M. Gabbay, M. Maglione, and G. Fantozzi, "Relaxation motion and possible memory of domain structures in barium titanate ceramics studied by mechanical and dielectric losses," J. Electroceram. **10**, 5–18 (2003).